Atmos. Chem. Phys. Discuss., 13, 10621–10660, 2013
www.atmos-chem-phys-discuss.net/13/10621/2013/
doi:10.5194/acpd-13-10621-2013

Atmospheric Chemistry and Physics Discussions

Four years of ground-based MAX-DOAS observations of HONO and NO_2 in the Beijing area

F. Hendrick[1], J.-F. Müller[1], K. Clémer[1,*], M. De Mazière[1], C. Fayt[1], C. Hermans[1], T. Stavrakou[1], T. Vlemmix[1,2], P. Wang[3], and M. Van Roozendael[1]

[1]Belgian Institute for Space Aeronomy (BIRA-IASB), Brussels, Belgium
[2]Delft University of Technology (TU-Delft), Delft, the Netherlands
[3]Institute of Atmospheric Physics, Chinese Academy of Science, Beijing, China
[*]now at: Instituut voor Sterrenkunde, Katholieke Universiteit Leuven, Leuven, Belgium

Received: 26 March 2013 – Accepted: 12 April 2013 – Published: 22 April 2013

Correspondence to: F. Hendrick (franch@oma.be)

Published by Copernicus Publications on behalf of the European Geosciences Union.

Abstract

Ground-based Multi-Axis Differential Optical Absorption Spectroscopy (MAX-DOAS) measurements of nitrous acid (HONO) and its precursor NO_2 (nitrogen dioxide) have been performed daily in Beijing city center (39.98° N, 116.38° E) from July 2008 to April 2009 and at the suburban site of Xianghe (39.75° N, 116.96° E) located ~60 km east of Beijing from March 2010 to December 2012. This extensive data set allowed for the first time the investigation of the seasonal cycle of HONO as well as its diurnal variation in and in the vicinity of a megacity. Our study was focused on the HONO and NO_2 near-surface concentrations (0–200 m layer) and total vertical column densities (VCDs) retrieved by applying the Optimal Estimation Method to the MAX-DOAS observations. Monthly averaged HONO near-surface concentrations at local noon display a strong seasonal cycle with a maximum in late fall/winter (~0.8 and 0.7 ppb at Beijing and Xianghe, respectively) and a minimum in summer (~0.1 ppb at Beijing and 0.03 ppb at Xianghe). The seasonal cycles of HONO and NO_2 appear to be highly correlated, with correlation coefficients in the 0.7–0.9 and 0.5–0.8 ranges at Beijing and Xianghe, respectively. The stronger correlation of HONO with NO_2 and also with aerosols observed in Beijing suggests possibly larger role of NO_2 conversion into HONO in the Beijing city center than at Xianghe. The observed diurnal cycle of HONO near-surface concentration shows a maximum in the early morning (about 1 ppb at both sites) likely resulting from night-time accumulation, followed by a decrease to values of about 0.1–0.4 ppb around local noon. The HONO/NO_2 ratio shows a similar pattern with a maximum in the early morning (values up to 0.08) and a decrease to ~0.01–0.02 around local noon. The seasonal and diurnal cycles of the HONO near-surface concentration are found to be similar in shape and in relative amplitude to the corresponding cycles of the HONO total VCD and are therefore likely mainly driven by the balance between HONO sources and the photolytic sink, whereas dilution effects appear to play only a minor role. The estimation of OH radical production from HONO and O_3 photolysis based on retrieved HONO near-surface concentrations and calculated photolysis rates

ACPD
13, 10621–10660, 2013

indicate that HONO is by far the largest source of OH radicals in winter as well as in the early morning at all seasons, while the contribution of O_3 dominates in summer from mid-morning until mid-afternoon.

1 Introduction

Since the late 1970s, nitrous acid (HONO) has been identified as a key chemical species in the troposphere, especially through its photolysis which leads to the formation of the hydroxyl radical OH (Perner and Platt, 1979). OH is known as the major oxidant ("detergent") of the atmosphere responsible for the degradation of most pollutants. It contributes also to the formation of ozone and PANs (peroxyacyl nitrates) causing the so-called "photochemical smog" in polluted regions, as well as to the formation of aerosol particles from the oxidation of volatile organic compounds (VOCs). The photochemistry of HONO has been and is still extensively discussed in the literature (see e.g., Sörgel et al., 2011a; Li et al., 2012; and Elshorbany et al., 2012). The heterogeneous conversion of nitrogen dioxide (NO_2) on wet organic and inorganic ground surfaces (soil, buildings, vegetation, and aerosols) is believed to be a major source of HONO, and very probably its main source during the night (Wojtal et al., 2011 and references therein):

$$2NO_2 + H_2O + \text{surface} \rightarrow HONO + HNO_3 \quad \text{(R1)}$$

Recent field studies and laboratory measurements have identified other heterogeneous daytime sources like photosensitized reduction of NO_2 on organic surfaces (George et al., 2005; Stemmler et al., 2006) and the photolysis of adsorbed nitric acid/nitrate at UV wavelengths (Zhou et al., 2003). Su et al. (2011) also showed that soil, through nitrite-producing microbes, can release important HONO amounts. Other HONO sources are direct emissions from combustion processes and the following gas-phase reaction:

$$NO + OH + M \rightarrow HONO + M \quad \text{(R2)}$$

ACPD
13, 10621–10660, 2013

Reaction (R2) operates only during daytime, when the OH and NO concentrations are high. HONO sinks include dry deposition during nighttime, and photolysis (Reaction R3) during daytime, at a rate close to $10^{-3}\,s^{-1}$ around noon (see Sect. 3.3):

$$HONO + h\nu(\lambda<400\,nm) \rightarrow OH + NO \quad (R3)$$

$$HONO + OH \rightarrow H_2O + NO_2 \quad (R4)$$

The reaction of HONO with OH (Reaction R4) is comparatively very slow. The rapid photolysis of HONO accumulated during the night is the main source of OH radicals in early morning when other radical sources, i.e. the photolysis of ozone and carbonyls, are still weak. It should be noted that recent measurements in the Los Angeles Basin have suggested that nitryl chloride ($ClNO_2$) can be, together with HONO, an important source of radicals in the morning in urban environments (Young et al., 2012). This study also showed that vertical gradients of radical precursors should be taken into account in radical budgets, especially in case of HONO.

Despite the numerous field campaigns and laboratory experiments conducted during the last three decades, the main HONO formation mechanisms are still not fully characterized, and their relative contributions to the observed HONO concentrations are not well quantified. Model simulations accounting only for anthropogenic emissions and the known gas phase formation through Reaction (R2) generally largely underestimate the measured daytime HONO levels, with possibly important consequences for the prediction of oxidants (OH, O_3, PANs) (e.g., Kleffmann et al., 2005; Sörgel et al., 2011b). Consequently, the largely unknown HONO daytime source can have a significant impact on air quality and chemistry-climate modeling (Elshorbany et al., 2012 and references therein).

So far, HONO has been measured mainly using the long-path DOAS (Differential Optical Absorption Spectroscopy) and in-situ LOPAP-like (Long-Path Absorption Photometer) techniques. LOPAP is a wet chemical technique based on the dissolution of HONO in the liquid phase as nitrite (NO_2^-) followed by its detection as an azo dye (compound bearing the R-N=N-R′ functional group) with a long-path absorption photometer

ACPD
13, 10621–10660, 2013

(Heland et al., 2001; Kleffmann et al., 2002). The LOPAP instruments can generally be operated only for a limited period of time, from a few weeks to a couple of months, due to instrumental and logistics issues. Long-path DOAS is an active (i.e. using an artificial light source) DOAS technique consisting of the measurement of the trace gas concentration integrated along a light path of several hundred meters to a few kilometers between the light source and the spectrometer (Hönninger et al., 2004; Platt and Stutz, 2008). The first detection of HONO by long-path DOAS was made over the Los Angeles air basin in the late 1970s (Perner and Platt, 1979). Both long-path DOAS and LOPAP show a high sensitivity to HONO and have the advantage to be independent of daylight, enabling nighttime measurements.

Here we present four years of ground-based Multi-Axis (MAX-) DOAS observations of HONO and its main precursor NO_2 in the Beijing area from July 2008 till December 2012. It is the first time that measurements of HONO in or in the vicinity of a megacity are reported over such a long time period, allowing investigation of the seasonal variation of this species in urban conditions. In contrast to long-path DOAS, MAX-DOAS is a passive DOAS technique based on measurements of scattered sunlight at zenith and at different elevation angles towards the horizon (the so-called off-axis geometry), increasing therefore the sensitivity to absorbers present close to the ground such as HONO or NO_2 (Hönninger et al., 2004; Platt and Stutz, 2008). Due to the use of daylight and the need to minimize the contribution of the stratosphere for absorbers with strong stratospheric concentration like NO_2 here, our MAX-DOAS observations are performed from $\sim 85^\circ$ SZA (solar zenith angle) sunrise to 85° SZA sunset with a time resolution of ~ 15 min (time needed for a complete MAX-DOAS scan). The instrumental set up including data transfer is fully automated, allowing continuous daily operation throughout the year. Moreover, by applying appropriate inversion methods like the Optimal Estimation (OEM; Rodgers, 2000), some information on the vertical distribution of the target trace gases can be retrieved in addition to the vertical column density (e.g., Hendrick et al., 2004; Hönninger et al., 2004; Wittrock et al., 2004; Friess et al., 2006; Clémer et al., 2010; Vlemmix et al., 2011). It should be noted that

ACPD
13, 10621–10660, 2013

altitude-resolved measurements of trace gases are also possible with long-path DOAS or in-situ techniques, generally with a better vertical resolution and signal-to-noise ratio than MAX-DOAS, but these require more sophisticated instrumental set up like e.g. placing retro-reflectors or in-situ instruments on different floors of a building (e.g. Stutz et al., 2002; Wang et al., 2006; Wong et al., 2012; Villena et al., 2011).

In the present study, MAX-DOAS observations of HONO and NO_2 have been performed from July 2008 to April 2009 in the Beijing city center (39.98° N, 116.38° E) and from March 2010 until December 2012 at the suburban site of Xianghe (39.75° N, 116.96° E) located ~60 km east of Beijing. From these data sets, the diurnal and seasonal variations of the HONO and NO_2 vertical column densities (VCD) and near-surface concentrations in the Beijing area are investigated. The OH production from HONO is also estimated based on the retrieved HONO concentrations and calculated photolysis rates. In Sect. 2, the MAX-DOAS measurements of HONO and NO_2 are introduced, including a description of the instrumental set up, DOAS analysis settings, and vertical profile retrievals. Section 3 presents the results: the seasonal variation of daytime HONO and NO_2 VCDs and near-surface concentrations, their diurnal variation and an estimation of the OH production from HONO and ozone. Concluding remarks are given in the last section.

2 MAX-DOAS measurements

2.1 Instrumental set up

The MAX-DOAS instrument used in this study has been extensively described in Clémer et al. (2010). It is a dual-channel system composed of two grating spectrometers covering the UV and visible wavelength ranges (300–390 nm and 400–720 nm, respectively). The output of both spectrometers is connected to cooled CCD detectors. The spectrometers and detectors are mounted inside a thermo-regulated box in order to minimize thermal stress on optical and mechanical parts. The instrument function is

ACPD
13, 10621–10660, 2013

close to a Gaussian with a full width at half maximum (FWHM) of 0.4 nm and 0.9 nm for the UV and visible channels, respectively. Scattered light is collected at various elevation and azimuth angles by an optical head mounted on a commercial sun tracker (INTRA, Brusag) and the light is guided to the two spectrometers through optical fibers.

The instrument, which was designed and assembled at BIRA-IASB in Brussels, was installed during the July 2008–April 2009 period on the roof of the Institute of Atmospheric Physics (IAP) of the Chinese Academy of Sciences located in the Beijing city center (39.98° N, 116.38° E). Then, it was moved to the suburban site of Xianghe (39.75° N, 116.96° E) located about 60 km east of Beijing where it has been operating continuously from March 2010 until now. At both locations, the telescope points towards a fixed azimuth direction (north) and a full MAX-DOAS scan, which requires ~ 15 min, comprises the following 9 elevation angles: 2°, 4°, 6°, 8°, 10°, 12°, 15°, 30°, and 90° (zenith).

2.2 DOAS analysis

The measured scattered light spectra are analyzed using the spectral fitting software suite QDOAS developed at BIRA-IASB (http://uv-vis.aeronomie.be/software/QDOAS/). The principle of the DOAS technique is to separate the absorption of molecular species which usually display narrow features from a broadband background resulting mainly from Mie and Rayleigh scattering and instrumental effects (Platt and Stutz, 2008). The direct product of the DOAS spectral fitting method is the differential slant column density (DSCD) which is the concentration of a given absorber integrated along the effective light path relative to the amount of the same absorber in a measured reference spectrum. For profile retrieval in the troposphere, it is a common way to select the zenith measurement of a MAX-DOAS scan as the reference for the off-axis DSCDs of the same scan in order to minimize the stratospheric signal (Clémer et al., 2010; Peters et al., 2012). This is particularly important for NO_2 which displays a significant concentration in the stratosphere.

ACPD
13, 10621–10660, 2013

HONO DSCDs are retrieved in the 337–375 nm wavelength range, taking into account the spectral signature of NO_2 at 220 and 296 K (Vandaele et al., 1998), O_3 at 218 and 243 K (Brion et al., 2004), O_4 (Hermans et al., 2003), BrO at 223 K (Fleischmann et al., 2004), HCHO at 293 K (Meller and Moortgat, 2000), and the filling-in of the solar Fraunhofer bands by the Ring effect (Grainger and Ring, 1962). The HONO absorption cross-sections at 296 K are obtained from Stutz et al. (2000). A fifth-order polynomial is used to fit the low frequency spectral structure due to molecular and Mie scattering. An example of DOAS fit for HONO is presented in Fig. 1.

In the case of NO_2, the 425–490 nm fitting window is used and, in addition to the NO_2 cross-sections at 220 and 296 K (Vandaele et al., 1998), the following trace gas cross-sections are taken into account in the DOAS analysis: O_3 at 241 K (Burrows et al., 1999), O_4 (Hermans et al., 2003), and H_2O (Harder and Brault, 1997). A Ring spectrum and a third-order polynomial closure term are also included. An example of DOAS fit for NO_2 is also shown in Fig. 1.

The O_4 DSCDs needed for the aerosol extinction profile retrieval (see Sect. 2.3) are retrieved in the UV and visible regions (338–370 nm and 425–490 nm, respectively) using the O_4 cross-sections from Hermans et al. (2003). The other DOAS settings are described in Clémer et al. (2010).

2.3 HONO and NO_2 profile retrievals

HONO and NO_2 vertical profiles can be retrieved for each MAX-DOAS scan by applying an inversion algorithm to the corresponding sets of DSCDs measured at the different elevation angles. This profiling technique is based on the fact that the mean scattering height rises into the atmosphere with the increase of the elevation angle and probes the layers where the tropospheric absorber is present. So, each measured DSCD of a MAX-DOAS scan is representative of the absorber concentration in a given altitude range and therefore the observed DSCD variation as a function of the elevation angle depends on the vertical distribution of the absorber. In this study, we used the bePRO inversion algorithm developed at BIRA-IASB (Clémer et al., 2010). It is based on

ACPD
13, 10621–10660, 2013

the Optimal Estimation Method (OEM; Rodgers, 2000) and uses a two-step approach. First, the aerosol extinction vertical profiles are retrieved at 360 and 477 nm for each MAX-DOAS scan from the corresponding measured O_4 DSCDs. The principle of this retrieval is the following: since the O_4 vertical profile is well-known and nearly constant (it varies with the square of the O_2 monomer concentration), O_4 DSCD measurements can provide information on the vertical distribution of aerosols (Wagner et al., 2004; Friess et al., 2006). This first step is required since the light path length through the atmosphere (and thus the measured HONO or NO_2DSCD) strongly depends on the aerosols and therefore a good estimate of the vertical distribution of the aerosols is needed to perform accurate HONO and NO_2 profile retrievals. Further details regarding our aerosol retrieval (aerosol optical depth (AOD) and extinction coefficient), including the corresponding bePRO settings, are extensively described in Clémer et al. (2010). In the second step, the bePRO algorithm is applied to the measured HONO and NO_2 DSCDs in order to retrieve vertical profiles of these trace gas species. In the OEM, the weighting function matrix (**K**) and the a priori profile x_a are two important retrieval parameters. **K** expresses the sensitivity of the measurements (DSCDs) to changes in the trace gas profile and it is calculated using the linearized discrete ordinate radiative transfer model (LIDORT; Spurr, 2008) as forward model. This code includes an analytical calculation of the weighting functions allowing for near real time automated retrievals without the need of pre-calculated look-up tables. Since the present retrieval problem is ill-conditioned (no unique solution for the trace gas or aerosol extinction vertical profile due to the too small information content of fitted DSCDs from one MAX-DOAS scan), a priori constraints are needed to reject unrealistic solutions and to stabilize the inversion. For HONO and NO_2 vertical profile retrievals, exponentially decreasing a priori profiles have been used with a fixed scaling height of 0.5 km according to the following expression:

$$x_a(z) = \frac{VCD_a}{SH} e^{-\frac{z}{SH}} \quad (1)$$

ACPD
13, 10621–10660, 2013

where $x_a(z)$ is the a priori profile (HONO or NO_2 concentration as a function of the altitude z), SH is the scaling height (fixed to 0.5 km) and VCD_a is the a priori vertical column density of HONO or NO_2. For each scan, VCD_a is derived using the geometrical approximation, i.e. the HONO or NO_2 layer is assumed to be located below the scattering altitude at 30° elevation, so that tropospheric HONO or NO_2 VCDs can be derived by applying a geometrical AMF to measured DSCDs at 30° elevation (Hönninger et al., 2004; Brinksma et al., 2008).

The other important retrieval parameter settings, which are the a priori and measurement uncertainty covariance matrices (S_a and S_ε, respectively), have been constructed as in Clémer et al. (2010). Profile retrievals have been performed at the following wavelengths: 354 nm for HONO and 460 nm for NO_2. The pressure and temperature profiles were taken from the US Standard Atmosphere and the retrieval grid was chosen as in Clémer et al. (2010): ten layers of 200 m thickness between 0 and 2 km, two layers of 500 m between 2 and 3 km and 1 layer between 3 and 4 km.

Typical examples of HONO and NO_2 vertical profile retrievals are presented in Figs. 2 and 3, respectively. The examination of the averaging kernels, which give information on the sensitivity of the measurements to the vertical distribution, shows that for low and moderate aerosol contents, the HONO retrieval is mostly sensitive close to the surface (0–200 m layer) and to the overhead column above 200 m. In the case of NO_2, three layers can be distinguished: 0–200 m, 200–400 m, and the column above 400 m. Since our study is mainly focused on HONO, we decided to investigate the HONO and NO_2 concentrations in the 0–200 m layer as well as the vertical column densities of these species. The retrieval of both columns and near-surface concentrations is the main strength of the MAX-DOAS technique: it helps to distinguish between photochemical and vertical transport influences on the diurnal cycle of HONO and NO_2 given that columns are less sensitive than concentrations to the growth of the boundary layer. Regarding the information content, it should be noted that the number of independent pieces of information, also called degrees of freedom for signal (DOFS) and given by the trace of the matrix **A** (Rodgers, 2000), is generally larger for NO_2 than for HONO

ACPD
13, 10621–10660, 2013

(2.8 and 1.6 in the examples shown in Figs. 2 and 3). This is due to the fact that the NO_2 concentration is larger by more than one order of magnitude than the HONO concentration, leading to a significantly higher sensitivity of the MAX-DOAS observations to NO_2.

From the error budgets presented in Figs. 2 and 3, the smoothing error, which represents the difference between the retrieved profile and the true profile due to vertical smoothing by the retrieval algorithm (Rodgers, 2000), is seen to be the dominant contribution to the total error except in the lowest layers. The total retrieval errors on the HONO volume mixing ratio (VMR) in the 0–200 m layer and on the HONO vertical columns amount on average to 19 % and 8 %, respectively at Beijing and to 23 % and 10 % at Xianghe. The corresponding values for NO_2 are 4 % and 2.5 %, respectively at Beijing and 8 % and 2.5 % at Xianghe. As in Clémer et al. (2010), the forward model parameters error has been neglected in the calculation of the error budget. The uncertainty related to the choice of the a priori profile for the HONO and NO_2 retrievals has been estimated by varying the scaling height (SH; see Eq. 1) defining the a priori profile, more precisely, by adopting a value of either 0.5 km (standard retrieval) or 1 km. At Beijing, using a SH value of 1 km instead of 0.5 km leads to the following average changes on the retrieved quantities: −7 and +10 % on the HONO and NO_2 near-surface concentrations, respectively, and +20 and +10 % on the HONO and NO_2 vertical columns, respectively. The corresponding changes for Xianghe are +11 and +14 % (HONO and NO_2 near-surface concentrations) and +23 and +10 % (HONO and NO_2 vertical columns). Total uncertainties are estimated by combining the above error sources to the systematic uncertainty on the HONO and NO_2 cross-sections (5 % and 3 %, respectively, according to Stutz et al., 2000; Vandaele et al., 1998). The error budget on HONO and NO_2 near-surface concentrations and vertical column densities is presented in Table 1.

It is known that clouds and aerosols might bias the MAX-DOAS trace gas retrieval (Wagner et al., 2004; Friess et al., 2006). Instead of explicitly applying a could filtering approach, HONO, NO_2, and aerosol profile retrievals have been quality-checked for

ACPD
13, 10621–10660, 2013

each MAX-DOAS scan by comparing the measured DSCDs to those calculated using the retrieved profiles (see examples of retrieval fit results in Figs. 2 and 3 for HONO and NO_2). In practice, the selection of good profile retrievals is based on the following criteria: Eq. (1) residual (RMS) of the retrieval fit smaller than an empirically derived threshold value (3.5×10^{14} molec cm^{-2} for HONO and 2.4×10^{16} molec cm^{-2} for NO_2), (2) DOFS larger than 0.7 meaning that the information comes mainly from the measurements and not from the a priori profile, and (3) scans with bad O_4 fit results (RMS of the fit larger than 30 % of the mean O_4 DSCD of the scan), which can be obtained e.g. for changing aerosol loading or/and cloud conditions during a scan, are rejected.

3 Results and discussion

3.1 Seasonal variation of daytime HONO and NO_2

Time-series of HONO and NO_2 surface concentration and VCD monthly means at local noon are presented in Fig. 4. A marked seasonality of the HONO surface concentration and VCD is observed at both stations, with a maximum in late fall/winter and a minimum in summer. The HONO surface concentration (0–200 m layer) ranges between $\sim$ 0.1 and 0.8 ppb in Beijing and between $\sim$ 0.03 and 0.7 ppb in Xianghe. These values are consistent with published daytime surface measurements of HONO performed in or in the vicinity of big cities and ranging from 0.05 to 2 ppb (Li et al., 2012), the lowest and highest values having been observed in Tokyo (Kanaya et al., 2007) and in Guangzhou City, South China (Qin et al., 2009), respectively. From Fig. 4, we see that the HONO seasonal variation follows well the seasonality of NO_2 which is believed to be its main precursor. The late fall/winter maximum is a well-known feature of NO_2 columns over industrialized areas at mid-latitudes and in particular over Northeastern China (Richter et al., 2005) and is mainly attributed to the longer photochemical lifetimes caused by the winter depletion of OH radical levels (Stavrakou et al., 2013). Domestic heating also contributes to the late fall/winter maximum, but its role is minor due to the dominance

ACPD
13, 10621–10660, 2013

of other NO_x sources in Eastern China (Zhang et al., 2007). The HONO seasonality is the result of both enhanced production in winter (due to the NO_2 maximum) and more efficient photolysis in summer. Furthermore, the boundary layer height (BLH) is higher in summer than in winter, about 3 and 1 km in summer and winter, respectively, according to ECMWF ERA-Interim data, leading to a larger dilution of HONO in summer and therefore to lower concentrations close to the surface. This effect seems minor, however, since the seasonal cycle of HONO VCD has an only slightly lower relative amplitude (peak-to-trough ratio between 5 and 10) compared to the near-surface concentration (ratio around 10) (see Fig. 4).

The HONO and NO_2 seasonal variations at both stations are further illustrated in Fig. 5 where the monthly near-surface concentrations and VCDs around local noon have been averaged over the whole measurement period. The HONO concentrations and columns are found to be generally larger at Beijing than at Xianghe, as a result of the larger NO_2 concentrations observed in the Beijing city center (Figs. 4 and 5). The largest difference between the sites concerns the 90th percentile of HONO surface concentrations (Fig. 5) which can reach up to 2 ppb at Beijing in winter while the corresponding values do not exceed 1.25 ppb for the same period at Xianghe. The heterogeneous conversion of NO_2 into HONO appears to be very probably the dominant source of HONO at both sites and especially in Beijing, given the high correlation coefficient found between HONO and NO_2 near-surface concentrations (R_{HONO/NO_2}) and between HONO concentration and the aerosol extinction coefficient ($R_{HONO/AERO}$) retrieved in the 0–200 m layer from simultaneous O_4 MAX-DOAS measurements (see Sect. 2.3). Figure 6 shows that R_{HONO/NO_2} lies in the range 0.7–0.9 at Beijing and 0.5–0.8 at Xianghe, while the corresponding $R_{HONO/AERO}$ values are comprised between 0.75 and 0.95 and between 0.55 and 0.85, respectively. Similar correlation coefficient values are obtained between integrated concentrations, i.e. between HONO and NO_2 VCDs and between HONO VCD and retrieved AOD (see Sect. 2.3), suggesting that the high correlation obtained for surface concentrations are not due to changes resulting from the variation of the boundary layer height. The strong correlation between HONO

ACPD
13, 10621–10660, 2013

and aerosols at both stations could be related to the high concentrations of PM_{10} and $PM_{2.5}$ usually observed in the Beijing area and making available large surface areas for heterogeneous reactions. This feature has been invoked by Li et al. (2011) to explain the large contribution (~ 60 %) of reactions on aerosols to the total HONO production in the Beijing region. This was estimated by comparing observations of HONO, O_3, PM_{10}, and $PM_{2.5}$ to meteorological-chemistry model simulations. A significant role played by PM_{10} is further supported by the high correlation coefficients derived by Qin et al. (2009) from long-path DOAS and particulate monitor measurements in summer in the Guangzhou city, China (R_{HONO/NO_2} and $R_{HONO/PM10}$ close or larger than 0.7). In contrast, our R_{HONO/NO_2} and $R_{HONO/AERO}$ correlation coefficients are significantly higher than those reported by Li et al. (2012) at a rural site in Southern China in summer ($R_{HONO/NO_2} \sim 0.4$ and $R_{HONO/AERO} \sim 0.6$), confirming that the formation of HONO from NO_2 is more dominant in an urban environment, while other sources (e.g. soil emissions or the photolysis of nitrate and nitric acid deposited on vegetation) appear to play a larger role in rural areas.

The seasonal variation of the ratio of HONO and NO_2 concentrations (HONO/NO_2) at local noon is shown in Fig. 6, and the season-averaged concentrations, vertical columns and ratios are summarized in Tables 2 and 3. The scaling of HONO to NO_2 or NO_x is often used to make the link between HONO and its possible sources, i.e. as an indicator of the efficiency of the conversion of NO_2 into HONO (e.g. Sörgel et al., 2011a; Wojtal et al., 2011; Li et al., 2012). The HONO/NO_2 ratio values are usually sorted into the three following regimes (Wojtal et al., 2011 and references therein): direct emission (HONO/NO_2less than 0.01) and surface sources in low and high relative humidity environments (HONO/NO_2 in the 0.01–0.03 and 0.03–0.1 ranges, respectively). It should be noted that HONO/NO_2 ratio values up to 0.30 have been derived from nighttime long-path DOAS measurements in Kathmandu, Nepal by Yu et al. (2009) and were explained by high pollution and relative humidity and low inversion layer. The monthly averaged HONO/NO_2 ratio observed in the 0–200 m layer is comprised on average between 0.007 and 0.028 at both sites (Fig. 6). Although there are significant differences

ACPD
13, 10621–10660, 2013

(up to a factor of 2) between the near-surface concentrations ratios observed at Beijing and Xianghe, the VCD ratios are remarkably similar at both sites, and show only little seasonal variations, with values varying between 0.008 in summer and 0.013 in fall and winter (see Table 3). The summertime minimum is consistent with the higher photolytic sink in that season. Higher ratio values are obtained in the 0–200 m layer, by a factor ranging between 1.5 and 2, due to the shorter HONO lifetime and hence the stronger vertical gradients for HONO compared to NO_2 (see e.g. Figs. 2 and 3). Although the photolytic loss of HONO is likely an important driver of these daytime HONO/NO_2 ratios, differences between the seasonal variations of the near-surface concentration ratios at both sites are observed (see Fig. 6), suggesting that other processes can play a significant role. These could be e.g. differences in vertical mixing or effects of horizontal transport of NO_2, especially during the winter when lifetimes are long. The 90th percentile of the monthly-averaged near-surface HONO/NO_2 ratios indicates that this ratio can reach values of up to about 0.05 at both sites (Fig. 6). The mean and 90th percentile values reported here are consistent with those measured around local noon in big cities and ranging from 0.003 to 0.075 (Li et al., 2012; Elshorbany et al., 2012, and references therein).

3.2 Diurnal variation of HONO and NO_2

Since the MAX-DOAS instrument operates continuously from about 85° SZA sunrise to 85° SZA sunset with a time resolution of ∼15 min, the diurnal variation of HONO and NO_2 surface concentrations and VCDs can be thoroughly investigated throughout the year at both stations. Figure 7 presents the diurnal variation of HONO and NO_2 surface concentrations and of HONO/NO_2 ratios observed at Beijing and Xianghe. Measurements have been averaged per season using 1 h bins.

The diurnal cycle of NO_2 reflects the balance between anthropogenic emissions and photochemical sinks. In fall/winter, when photochemical activity is weak, accumulation of NO_2 results in a continuous increase of its concentrations during the day, whereas in spring/summer, the diurnal cycle is relatively flat. The diurnal cycle of the HONO

ACPD
13, 10621–10660, 2013

concentration in the 0–200 m layer exhibits a maximum in the early morning (1.3–1.6 ppb and 0.7–1.0 ppb at Beijing and Xianghe, respectively) due to the nighttime build-up, followed by a decrease. This decrease continues throughout the day at both stations in fall/winter, while in spring/summer the HONO concentration remains relatively constant from local noon until ∼ 4 p.m., after which time HONO increases slightly until sunset. This diurnal cycle shape is similar to the cycle observed in several field campaigns (Qin et al., 2009; Li et al., 2012; Elshorbany et al., 2012, and references therein). The morning decrease can be attributed to the increasing HONO photolysis rates and vertical mixing, while the HONO increase in the late afternoon can be caused by the progressive absence of photolytic loss and the decrease of the boundary layer height. However, since the HONO VCD has a very similar diurnal cycle (see Fig. 8), the surface concentration variation during the day is therefore not driven by dilution effects. This is consistent with the study of Qin et al. (2009) which indicated a higher correlation between HONO and NO_2 at Guangzhou than between HONO and CO, the latter being used as a tracer for the transport processes. It should be noted that the NO_2 VCD diurnal cycles averaged per season at Beijing (see Fig. 8) have been compared to those measured in the Beijing city center during the 2008–2011 period by Ma et al. (2013) using also the MAX-DOAS technique. Both NO_2 VCD data sets are found to agree well in fall and winter (correlation coefficients of 0.6 and 0.9, respectively) but not in spring and summer (correlation coefficients of −0.3 and 0.3, respectively). Further investigations beyond the scope of the present study would be needed to interpret these results.

As shown in Figs. 7 and 8, the HONO/NO_2 ratio has a marked diurnal cycle at both stations with, as for HONO, a maximum in the early morning (ratio values up to ∼ 0.05–0.08 in summer) and a decrease during daytime to values around 0.01–0.02. It should be noted that this diurnal cycle, with the absence of a significant increase of the HONO/NO_2 ratio around local noon, is very similar to the one derived by Qin et al. (2009) from long-path DOAS observations in Guangzhou city.

ACPD
13, 10621–10660, 2013

3.3 Estimation of OH production from HONO

In order to evaluate the importance of HONO as a source of OH radicals, especially compared to the contribution of O_3 photolysis, the OH production from HONO has been calculated in the 0–200 m layer at both stations from the retrieved HONO concentrations and simulated photolysis rates J (HONO). OH is formed from O_3 through the following reaction sequence:

$$O_3 + h\nu(\lambda<340\,\text{nm}) \rightarrow O(^1D) + O_2 \quad \text{(R5)}$$

$$O(^1D) + H_2O \rightarrow 2OH \quad \text{(R6)}$$

The corresponding OH production has been estimated from an assumed O_3 concentration fixed to 30 ppb, water vapor concentration from ECMWF (European Center for Medium-Range Weather Forecasts) ERA-Interim re-analysis fields (http://www.ecmwf.int/research/era/do/get/index), and simulated photolysis rate J ($O_3 \rightarrow O(^1D)$). Since the value of 30 ppb for O_3 is significantly smaller than the afternoon O_3 concentrations (up to 60 ppb) observed in summer (Lu et al., 2012; Wu et al., 2011), we tested the impact of using the diurnal cycle of O_3 measured by Chou et al. (2011) in the Beijing city center during CAREBeijing-2006. Photolysis rates have been calculated using the TUV package including the SDISORT radiative transfer code (Madronich and Hocke, 1998). The effects of clouds are ignored, whereas attenuation by aerosols is estimated from the aerosol optical depths retrieved by MAX-DOAS at Beijing and Xianghe (see Sect. 2.3), assuming a single scattering albedo equal to 0.9 and an asymmetry parameter equal to 0.7. The albedo is set to 0.05, except over snow (0.5). Snow presence and ozone total columns are obtained from ECMWF ERA-Interim fields.

The calculated photolysis rates are presented in Fig. 9. The J (HONO) values are consistent with those measured by Li et al. (2012) in the Pearl River Delta region in Southern China, and correspond to a noon photolytic lifetime of about 15–20 min, with little differences between the seasons. The diurnal cycles of OH production due to HONO and O_3 are depicted in Fig. 10. At both stations, the OH production from HONO in the 0–200 m layer exhibits a maximum in the morning, between 7 and 9 a.m.

ACPD
13, 10621–10660, 2013

in spring/summer and between 8 and 11 a.m. in fall/winter. This maximum is larger at Beijing than at Xianghe, with e.g. winter values reaching 1.2 ppb h^{-1} and 0.7 ppb h^{-1}, respectively, due to the generally larger HONO concentration observed in Beijing (Fig. 7). The shape of this diurnal cycle is similar to the one calculated by Sörgel et al. (2011b) from HONO measurements over a pine forest close to the industrial area of Huelva, Southwest Spain in fall. However, the maximum of OH production from HONO was significantly lower there ($\sim$ 0.2 ppb h^{-1}).

Comparison of the HONO and O_3 contributions to OH production reveals that HONO is the main contributor in all seasons except summer, with relative HONO contributions larger than 70 % (more than 90 % in winter) around 12:00–13:00 LT. In summer, the contribution of O_3 dominates between 09:30 LT and 16:00 LT with a maximum of 70 % around 13:00–14:00 LT. At Beijing, this feature is strengthened by considering the diurnal cycle of the ozone concentration measured by Chou et al. (2011) with high afternoon ozone mixing ratios, and very low values in the early morning. In that case, the contribution of O_3 to OH production reaches a maximum of 80 % in the early afternoon.

The seasonal variation of the HONO and O_3 contributions at local noon is displayed in Fig. 11. It is largely explained by the seasonal cycle of ozone photolysis rates (Fig. 9) and H_2O concentrations, which both maximize in summer. These results show that HONO is the main source of OH radicals in winter as well as in the early morning at all seasons in urban areas, in agreement with our current knowledge of the HONO photochemistry (see e.g. Li et al., 2012 and references therein).

4 Summary and conclusions

For the first time, the seasonal variation of HONO has been investigated in and in the vicinity of a megacity. This has been achieved using MAX-DOAS observations of HONO and its main precursor NO_2 in the Beijing city center and at the suburban site of Xianghe located $\sim$ 60 km east of Beijing. The MAX-DOAS spectrometers have the advantage that they can be operated year-round during daytime in a fully automated

ACPD
13, 10621–10660, 2013

way. Moreover, independent information on the near-surface concentration and vertical columns of trace gases can be retrieved from multiple elevation angle observations using dedicated inversion methods like the OEM used here. Our instrument was operated in the Beijing city center from July 2008 until April 2009, and in Xianghe from March 2010 until now. The total error on retrieved near-surface concentrations and vertical columns are comprised between 21 and 26 % for HONO and between 11 and 16 % for NO_2.

HONO and NO_2 concentrations retrieved at both stations around local noon in the 0–200 m layer exhibit the same marked seasonality, with a maximum in late fall/winter and a minimum in summer. The strong link between HONO and NO_2 is further supported by the high correlation of HONO with NO_2 found throughout the year, with coefficients comprised in the 0.7–0.9 and 0.5–0.8 ranges at Beijing and Xianghe, respectively. Like NO_2, HONO is more abundant at Beijing than at Xianghe, with mean VMR ranging from $\sim$ 0.1 to 0.8 ppb and from $\sim$ 0.03 to 0.7 ppb, respectively. These values are found to be consistent with previously reported daytime HONO measurements in urban conditions. A strong role of NO_2 conversion to HONO at Beijing is suggested from the higher correlation coefficients between HONO and aerosol extinctions retrieved in the 0–200 m layer at Beijing (ranging from 0.75 to 0.95 instead of 0.55 to 0.85 at Xianghe).

The diurnal profiles of HONO surface concentration and vertical column show a maximum in the early morning (1.3–1.6 ppb/1.5–1.8 $\times 10^{15}$ molec cm^{-2} in Beijing and 0.7–1.0 ppb/0.9–1.1 $\times 10^{15}$ molec cm^{-2} in Xianghe) likely explained by the photolysis of the HONO accumulated during the night. The subsequent decrease (to about 0.1–0.4 ppb for the concentration and 0.1–0.6 $\times 10^{15}$ molec cm^{-2} for the vertical column around local noon) results mostly from a balance between HONO sources and the photolytic sink. Dilution effects appear to play only a minor role, given the observed very similar diurnal cycle of the HONO vertical column, which is expected to be insensitive to vertical transport variations. The observed HONO/NO_2 ratio diurnal cycle is very similar at both Beijing and Xianghe with a maximum in the early morning (values up to 0.08) and subsequent decreases to values ranging between 0.01 and 0.02 around local noon.

ACPD
13, 10621–10660, 2013

The production of OH radicals from HONO and O_3 has been estimated from observed HONO near-surface concentrations and calculated photolysis rates. At both stations, HONO is found to be the main contributor to OH production, except in summer around local noon where the contribution of O_3 dominates. The diurnal cycle of the OH production from HONO shows a maximum in the morning between 7 and 11 a.m., depending on season, followed by a rapid decrease. This maximum is larger at Beijing than at Xianghe, especially in winter time where the OH production from HONO reaches $\sim 1.2\,\mathrm{ppb\,h^{-1}}$ and $\sim 0.7\,\mathrm{ppb\,h^{-1}}$, respectively.

To conclude, MAX-DOAS is shown to be a useful and reliable technique for monitoring HONO near-surface concentrations and vertical column amounts in polluted areas. Multi-year data sets of HONO observations, such presented in this work, offer a better quantitative characterization of HONO photochemistry and can provide additional constraints to modelling studies. For example, the diurnal and seasonal profiles of the $HONO/NO_2$ ratio derived in this study could be used in atmospheric models to constrain the rate of heterogeneous conversion of NO_2 to HONO, in order to investigate the possible effects of this HONO source on the budget of oxidants.

Acknowledgements. This research was financially supported at IASB-BIRA by the Belgian Federal Science Policy Office, Brussels (PRODEX contract A3C and AGACC-II project) and by the EU 7th Framework Programme projects NORS (contract 284421) and SHIVA (contract 226224). We also acknowledge M. Bauwens (BIRA-IASB) for her technical support.

References

Brion, J., Chakir, A., Charbonnier, J., Daumont, D., Parisse, C., and Malicet, J.: Absorption spectra measurements for the ozone molecule in the 350–830 nm region, J. Atmos. Chem., 30, 291–299, doi:10.1023/A:1006036924364, 2004.

Brinksma, E. J., Pinardi, G., Volten, H., Braak, R., Richter, A., Schönhardt, A., Van Roozendael, M., Fayt, C., Hermans, C., Dirksen, R. J., Vlemmix, T., Berkhout, A. J. C., Swart, D. P. J., Oetjen, H., Wittrock, F., Wagner, T., Ibrahim, O. W., de Leeuw, G., Moerman, M., Curier, R. L., Celarier, E. A., Cede, A., Knap, W. H., Veefkind, J. P., Eskes, H. J., Allaart, M., Rothe, R.,

ACPD
13, 10621–10660, 2013

Piters, A. J. M., and Levelt, P. F.: The 2005 and 2006 DANDELIONS NO_2 and aerosol intercomparison campaigns, J. Geophys. Res., 113, D16S46, doi:10.1029/2007JD008808, 2008.
Burrows, J. P., Richter, A., Dehn, A., Deters, B., Himmelmann, S., Voigt, S., and Orphal, J.: Atmospheric remote-sensing reference data from GOME – 2. Temperature-dependent absorption cross-sections of O_3 in the 231–794 nm range, J. Quant. Spectrosc. Ra., 61, 509–517, 1999.
Chou, C. C.-K., Tsai, C.-Y., Chang, C.-C., Lin, P.-H., Liu, S. C., and Zhu, T.: Photochemical production of ozone in Beijing during the 2008 Olympic Games, Atmos. Chem. Phys., 11, 9825–9837, doi:10.5194/acp-11-9825-2011, 2011.
Clémer, K., Van Roozendael, M., Fayt, C., Hendrick, F., Hermans, C., Pinardi, G., Spurr, R., Wang, P., and De Mazière, M.: Multiple wavelength retrieval of tropospheric aerosol optical properties from MAXDOAS measurements in Beijing, Atmos. Meas. Tech., 3, 863–878, doi:10.5194/amt-3-863-2010, 2010.
Elshorbany, Y. F., Steil, B., Brühl, C., and Lelieveld, J.: Impact of HONO on global atmospheric chemistry calculated with an empirical parameterization in the EMAC model, Atmos. Chem. Phys., 12, 9977–10000, doi:10.5194/acp-12-9977-2012, 2012.
Fleischmann, O. C., Hartmann, M., Burrows, J. P., and Orphal, J.: New ultraviolet absorption cross-sections of BrO at atmospheric temperatures measured by time-windowing Fourier transform spectroscopy, J. Photochem. Photobio. A, 168, 117–132, 2004.
Friess, U., Monks, P. S., Remedios, J. J., Rozanov, A., Sinreich, R., Wagner, T. and Platt, U.: MAX-DOAS O_4 measurements: a new technique to derive information on atmospheric aerosols: 2. Modeling studies, J. Geophys. Res., 111, D14203, doi:10.1029/2005JD006618, 2006.
George, C., Strekowski, R. S., Kleffmann, J., Stemmler, K., and Ammann, M.: Photoenhanced uptake of gaseous NO_2 on solid organic compounds: a photochemical source of HONO?, Faraday Discuss., 130, 195–210, doi:10.1039/B417888M, 2005.
Grainger, J. and Ring, J.: Anomalous Fraunhofer line profiles, Nature, 193, p. 762, 1962.
Harder, J. W. and Brault, J. W.: Atmospheric measurements of water vapor in the 442 nm region, J. Geophys. Res., 102, 6245–6252, 1997.
Heland, J., Kleffmann, J., Kurtenbach, R., and Wiesen, P.: A new instrument to measure gaseous nitrous acid (HONO) in the atmosphere, Environ. Sci. Technol., 35, 3207–3212, 2001.

ACPD
13, 10621–10660, 2013

Hendrick, F., Barret, B., Van Roozendael, M., Boesch, H., Butz, A., De Mazière, M., Goutail, F., Hermans, C., Lambert, J.-C., Pfeilsticker, K., and Pommereau, J.-P.: Retrieval of nitrogen dioxide stratospheric profiles from ground-based zenith-sky UV-visible observations: validation of the technique through correlative comparisons, Atmos. Chem. Phys., 4, 2091–2106, doi:10.5194/acp-4-2091-2004, 2004.

Hermans, C., Vandaele, A. C., Fally, S., Carleer, M., Colin, R., Coquart, B., Jenouvrier, A., and Mérienne, M.-F.: Absorption crosssection of the collision-induced bands of oxygen from the UV to the NIR, in: Proceedings of the NATO Advanced Research Workshop, Weakly Interacting Molecular Pairs: Unconventional Absorbers of Radiation in the Atmosphere, Fontevraud, France, 24 April–2 May 2002, edited by: Camy-Peyret, C. and Vigasin, A. A., NATO Science Series IV Earth and Environmental Sciences, vol. 27, Kluwer Academic Publishers, Boston, 193–202, 2003.

Hönninger, G., von Friedeburg, C., and Platt, U.: Multi axis differential optical absorption spectroscopy (MAX-DOAS), Atmos. Chem. Phys., 4, 231–254, doi:10.5194/acp-4-231-2004, 2004.

Kanaya, Y., Cao, R., Akimoto, H., Fukuda, M., Komazaki, Y., Yokouchi, Y., Koike, M., Tanimoto, H., Takegawa, N., and Kondo, Y.: Urban photochemistry in central Tokyo: 1. Observed and modeled OH and HO_2 radical concentrations during the winter and summer of 2004, J. Geophys. Res., 112, D21312, doi:10.1029/2007jd008670, 2007.

Kleffmann, J., Heland, J., Kurtenbach, R., Lörzer, J., and Wiesen, P.: A new instrument (LOPAP) for the detection of nitrous acid (HONO), Environ. Sci. Pollut. R., 4, 48–54, 2002.

Kleffmann, J., Gavriloaiei, T., Hofzumahaus, A., Holland, F., Koppmann, R., Rupp, L., Schlosser, E., Siese, M., and Wahner, A.: Daytime formation of nitrous acid: a major source of OH radicals in a forest, Geophys. Res. Lett., 32, L05818, doi:10.1029/2005GL022524, 2005.

Li, X., Brauers, T., Häseler, R., Bohn, B., Fuchs, H., Hofzumahaus, A., Holland, F., Lou, S., Lu, K. D., Rohrer, F., Hu, M., Zeng, L. M., Zhang, Y. H., Garland, R. M., Su, H., Nowak, A., Wiedensohler, A., Takegawa, N., Shao, M., and Wahner, A.: Exploring the atmospheric chemistry of nitrous acid (HONO) at a rural site in Southern China, Atmos. Chem. Phys., 12, 1497–1513, doi:10.5194/acp-12-1497-2012, 2012.

Li, Y., An, J., Min, M., Zhang, W., Wang, F., and Xie, P.: Impacts of HONO sources on the air quality in Beijing, Tianjin, and Hebei Province of China, Atmos. Environ., 45, 4735–4744, 2011.

ACPD
13, 10621–10660, 2013

Lu, K. D., Hofzumahaus, A., Holland, F., Bohn, B., Brauers, T., Fuchs, H., Hu, M., Häseler, R., Kita, K., Kondo, Y., Li, X., Lou, S. R., Oebel, A., Shao, M., Zeng, L. M., Wahner, A., Zhu, T., Zhang, Y. H., and Rohrer, F.: Missing OH source in a suburban environment near Beijing: observed and modelled OH and HO_2 concentrations in summer 2006, Atmos. Chem. Phys., 13, 1057–1080, doi:10.5194/acp-13-1057-2013, 2013.

Ma, J. Z., Beirle, S., Jin, J. L., Shaiganfar, R., Yan, P., and Wagner, T.: Tropospheric NO_2 vertical column densities over Beijing: results of the first three years of ground-based MAX-DOAS measurements (2008–2011) and satellite validation, Atmos. Chem. Phys., 13, 1547–1567, doi:10.5194/acp-13-1547-2013, 2013.

Madronich, S. and Flocke, S.: The role of solar radiation in atmospheric chemistry, in Handbook of Environmental Chemistry, edited by: Boule, P., Springer-Verlag, Heidelberg, 1–26, 1998.

Meller, R. and Moortgat, G. K.: Temperature dependence of the absorption cross sections of formaldehyde between 223 and 323 K in the wavelength range 225–375 nm, J. Geophys. Res., 105, 7089–7101, 2000.

Perner, D. and Platt, U.: Detection of nitrous acid in the atmosphere by differential optical absorption, Geophys. Res. Lett., 6, 917–920, 1979.

Peters, E., Wittrock, F., Großmann, K., Frieß, U., Richter, A., and Burrows, J. P.: Formaldehyde and nitrogen dioxide over the remote western Pacific Ocean: SCIAMACHY and GOME-2 validation using ship-based MAX-DOAS observations, Atmos. Chem. Phys., 12, 11179–11197, doi:10.5194/acp-12-11179-2012, 2012.

Platt, U. and Stuz, J.: Differential Optical Absorption Spectroscopy (DOAS), Principles and Applications, ISBN 978-3-540-21193-8, Springer, Berlin, Heidelberg, 2008.

Qin, M., Xie, P., Su, H., Gu, J., Peng, F., Li, S., Zeng, L., Liu, J., Liu, W., and Zhang, Y.: An observational study of the HONO-NO_2 coupling at an urban site in Guangzhou City, South China, Atmos. Environ., 43, 5731–5742, doi:10.1016/j.atmosenv.2009.08.017, 2009.

Richter, A., Burrows, J. P., Nüss, H., Granier, C., and Niemeier, U.: Increase in tropospheric nitrogen dioxide over China observed from space, Nature, 437, 129–132, doi:10.1038/nature04092, 2005.

Rodgers, C. D.: Inverse Methods for Atmospheric Sounding, Theory and Practice, World Scientific Publishing, Singapore, New Jersey, London, Hong Kong, 2000.

Sörgel, M., Trebs, I., Serafimovich, A., Moravek, A., Held, A., and Zetzsch, C.: Simultaneous HONO measurements in and above a forest canopy: influence of turbulent exchange on

ACPD
13, 10621–10660, 2013

mixing ratio differences, Atmos. Chem. Phys., 11, 841–855, doi:10.5194/acp-11-841-2011, 2011a.
Sörgel, M., Regelin, E., Bozem, H., Diesch, J.-M., Drewnick, F., Fischer, H., Harder, H., Held, A., Hosaynali-Beygi, Z., Martinez, M., and Zetzsch, C.: Quantification of the unknown HONO daytime source and its relation to NO_2, Atmos. Chem. Phys., 11, 10433–10447, doi:10.5194/acp-11-10433-2011, 2011b.
Spurr, R., LIDORT and VLIDORT: Linearized pseudo-spherical scalar and vector discrete ordinate radiative transfer models for use in remote sensing retrieval problems, Light Scattering Reviews, edited by: Kokhanovsky, A., Vol. 3, Springer, 2008.
Stavrakou, T., Müller, J.-F., Boersma, K. F., van der A, R. J., Kurokawa, J., Ohara, T., and Zhang, Q.: Key chemical NO_x sink uncertainties and how they influence top-down emissions of nitrogen oxides, Atmos. Chem. Phys. Discuss., 13, 7871–7929, doi:10.5194/acpd-13-7871-2013, 2013.
Stemmler, K., Ammann, M., Donders, C., Kleffmann, J., and George, C.: Photosensitized reduction of nitrogen dioxide on humic acid as a source of nitrous acid, Nature, 440, 195–198, doi:10.1038/nature04603, 2006.
Stutz, J., Kim., E. S., Platt, U., Bruno, P., Perrino, C., and Febo, A.: UV-vis absorption cross-section of nitrous acid, J. Geophys. Res., 105, 14585–14592, 2000.
Stutz, J., Alicke, B., and Neftel, A.: Nitrous acid formation in the urban atmosphere: gradient measurements of NO_2 and HONO over grass in Milan, Italy, J. Geophys. Res., 107, 8192, doi:10.1029/2001JD000390, 2002.
Su, H., Cheng, Y., Oswald, R., Behrendt, T., Trebs, I., Meixner, F. X., Andreae, M. O., Cheng, P., Zhang, Y., and Pöschl, U., Soil nitrite as a source of atmospheric HONO and OH radicals, Science, 333, 1616, doi:10.1126/science.1207687, 2011.
Vandaele, A. C., Hermans, C., Simon, P. C., Carleer, M., Colin, R., Fally, S., Mérienne, M.-F., Jenouvrier, A., and Coquart, B.: Measurements of the NO_2 absorption cross section from 42000 cm^{-1} to 10000 cm^{-1} (238–1000 nm) at 220 K and 294 K, J. Quant. Spectrosc. Ra., 59, 171–184, 1998.
Villena, G., Kleffmann, J., Kurtenbach, R., Wiesen, P., Lissi, E., Rubio, M., Croxatto, G., and Rappenglück, B.: Vertical gradients of HONO, NO_x and O_3 in Santiago de Chile, Atmos. Environ., 45, 3867–3873, doi:10.1016/j.atmosenv.2011.01.073, 2011.
Vlemmix, T., Piters, A. J. M., Berkhout, A. J. C., Gast, L. F. L., Wang, P., and Levelt, P. F.: Ability of the MAX-DOAS method to derive profile information for NO_2: can the boundary layer

ACPD
13, 10621–10660, 2013

and free troposphere be separated?, Atmos. Meas. Tech., 4, 2659–2684, doi:10.5194/amt-4-2659-2011, 2011.
Wagner, T., Dix, B., von Friedeburg, C., Friess, U., Sanghavi, S., Sinreich, R., and Platt, U.: MAX-DOAS O_4 measurements: a new technique to derive information on atmospheric aerosols – principles and information content, J. Geophys. Res., 109, D22205, doi:10.1029/2004JD004904, 2004.
Wittrock, F., Oetjen, H., Richter, A., Fietkau, S., Medeke, T., Rozanov, A., and Burrows, J. P.: MAX-DOAS measurements of atmospheric trace gases in Ny-Ålesund – Radiative transfer studies and their application, Atmos. Chem. Phys., 4, 955–966, doi:10.5194/acp-4-955-2004, 2004.
Wang, S., Ackermann, R., and Stutz, J.: Vertical profiles of O_3 and NO_x chemistry in the polluted nocturnal boundary layer in Phoenix, AZ: I. Field observations by long-path DOAS, Atmos. Chem. Phys., 6, 2671–2693, doi:10.5194/acp-6-2671-2006, 2006.
Wong, K. W., Tsai, C., Lefer, B., Haman, C., Grossberg, N., Brune, W. H., Ren, X., Luke, W., and Stutz, J.: Daytime HONO vertical gradients during SHARP 2009 in Houston, TX, Atmos. Chem. Phys., 12, 635–652, doi:10.5194/acp-12-635-2012, 2012.
Wojtal, P., Halla, J. D., and McLaren, R.: Pseudo steady states of HONO measured in the nocturnal marine boundary layer: a conceptual model for HONO formation on aqueous surfaces, Atmos. Chem. Phys., 11, 3243–3261, doi:10.5194/acp-11-3243-2011, 2011.
Wu, Q. Z., Wang, Z. F., Gbaguidi, A., Gao, C., Li, L. N., and Wang, W.: A numerical study of contributions to air pollution in Beijing during CAREBeijing-2006, Atmos. Chem. Phys., 11, 5997–6011, doi:10.5194/acp-11-5997-2011, 2011.
Young, C. J., Washenfelder, R. A., Roberts, J. M., Mielke, L. H., Osthoff, H. D., Tsai, C., Pikelnaya, O., Stutz, J., Veres, P. R., Cochran, A. K., VandenBoer, T. C., Flynn, J., Grossberg, N., Haman, C. L., Lefer, B., Stark, H., Graus, M., de Grouw, J., Gilman, J. B., Kuster, W. C., and Brown, S. S.: Vertically resolved measurements of nighttime radical reservoirs in Los Angeles and their contribution to the urban radical budget, Environ. Sci. Technol., 46, 10965–10973, doi:10.1021/es302206a, 2012.
Yu, Y., Galle, B., Panday, A., Hodson, E., Prinn, R., and Wang, S.: Observations of high rates of NO_2-HONO conversion in the nocturnal atmospheric boundary layer in Kathmandu, Nepal, Atmos. Chem. Phys., 9, 6401–6415, doi:10.5194/acp-9-6401-2009, 2009.
Zhang, Q., Streets, D. G., He, K., Wang, Y., Richter, A., Burrows, J. P., Uno, I., Jang, C. J., Chen, D., Yao, Z., and Lei, Y.: NO_x emission trends for China, 1995–2004:

ACPD
13, 10621–10660, 2013

the view from the ground and the view from space, J. Geophys. Res., 112, D22306, doi:10.1029/2007JD008684, 2007.

Zhou, X., Gao, H., He, Y., Huang, G., Bertman, S. B., Civerolo, K., and Schwab, J.: Nitric acid photolysis on surfaces in low-NO_x environments: significant atmospheric implications, Geophys. Res. Lett., 30, 2217, doi:10.1029/2003gl018620, 2003.

ACPD

13, 10621–10660, 2013

Table 1. Error budget of the retrieved HONO and NO_2 near-surface (0–200 m) concentrations and vertical column densities (VCD). The total uncertainty is calculated by adding the different error terms in Gaussian quadrature.

	Beijing				Xianghe			
	0–200 m		VCD		0–200 m		VCD	
	HONO	NO_2	HONO	NO_2	HONO	NO_2	HONO	NO_2
Total retrieval error (%)	19	4	8	2.5	23	8	10	2.5
Uncertainty related to the a priori (%)	7	10	20	10	11	14	23	10
Uncertainty on HONO or NO_2 cross sections (%)	5	3	5	3	5	3	5	3
Total uncertainty (%)	21	11	22	11	26	16	26	11

ACPD
13, 10621–10660, 2013

Table 2. Mean HONO near-surface concentration (VMR in ppb unit) and vertical column density (VCD in 10^{15} molec cm^{-2} unit) around local noon (±2 h) at Beijing and Xianghe. The 10th and 90th percentiles of the data are also given.

		Beijing			Xianghe		
		HONO mean	10th perc.	90th perc.	HONO mean	10th perc.	90th perc.
Spring	VMR	0.14	0.04	0.26	0.16	0.03	0.30
	VCD	0.26	0.16	0.39	0.25	0.09	0.41
Summer	VMR	0.19	0.01	0.42	0.09	0.01	0.21
	VCD	0.26	0.05	0.53	0.15	0.06	0.28
Fall	VMR	0.46	0.05	1.17	0.38	0.03	1.01
	VCD	0.59	0.14	1.42	0.48	0.10	1.15
Winter	VMR	0.48	0.04	1.04	0.34	0.02	0.86
	VCD	0.69	0.17	1.33	0.44	0.09	0.96

ACPD
13, 10621–10660, 2013

Table 3. Mean HONO/NO_2 ratio (VMR/VMR and VCD/VCD) around local noon (±2 h) at Beijing and Xianghe. The 10th and 90th percentiles of the data are also given.

		Beijing			Xianghe		
		HONO/NO_2 mean	10th perc.	90th perc.	HONO/NO_2 mean	10th perc.	90th perc.
Spring	VMR	0.015	0.005	0.024	0.024	0.006	0.046
	VCD	0.010	0.006	0.014	0.012	0.006	0.021
Summer	VMR	0.010	0.001	0.015	0.017	0.001	0.035
	VCD	0.008	0.005	0.014	0.009	0.004	0.015
Fall	VMR	0.020	0.007	0.037	0.018	0.006	0.033
	VCD	0.014	0.007	0.023	0.012	0.006	0.021
Winter	VMR	0.018	0.007	0.028	0.020	0.004	0.039
	VCD	0.013	0.007	0.021	0.012	0.005	0.022

ACPD
13, 10621–10660, 2013

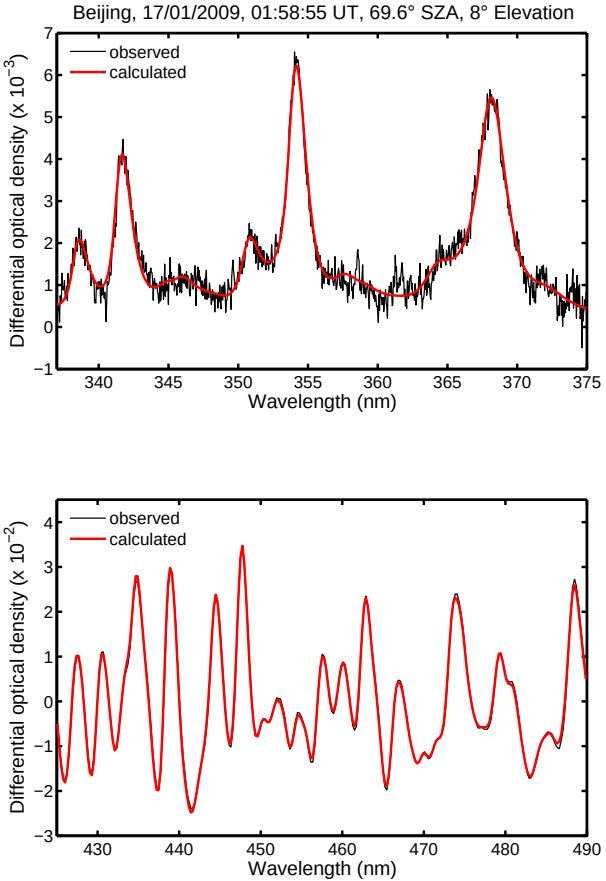

Fig. 1. Example of DOAS fit for HONO (upper plot) and NO_2 (lower plot) at Beijing. Similar DOAS fit results are obtained at Xianghe.

ACPD
13, 10621–10660, 2013

MAX-DOAS observations of HONO and NO_2 in the Beijing area

F. Hendrick et al.

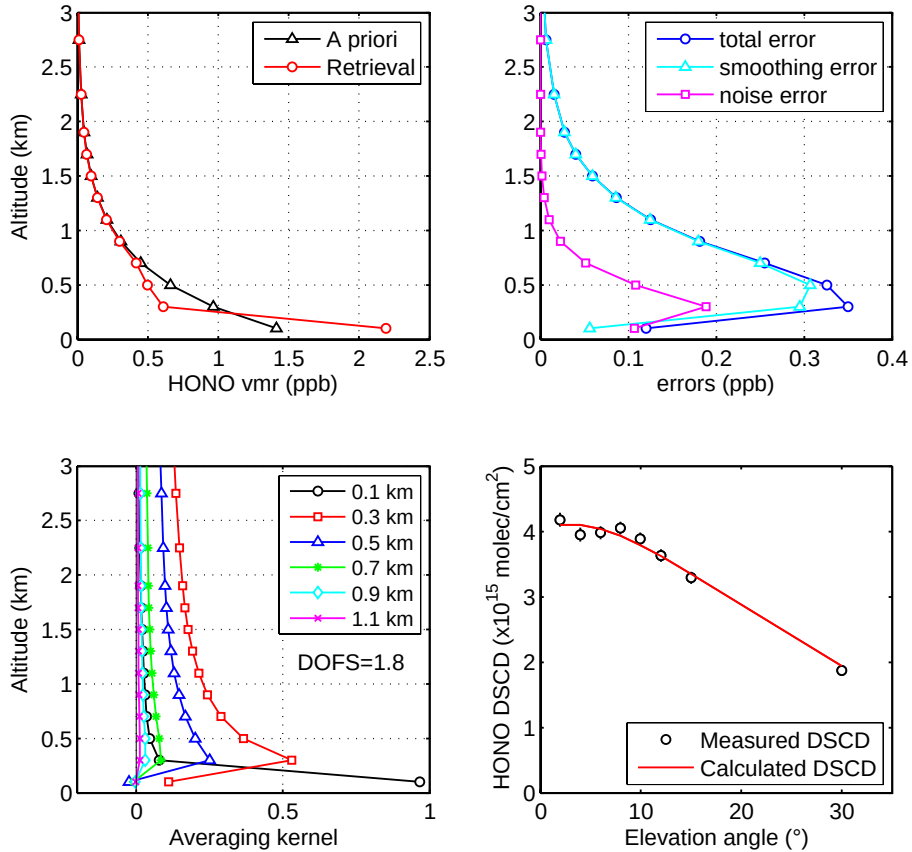

Fig. 2. Typical example of HONO vertical profile retrieval (Beijing, 21 January 2009, ~ 10:15 LT). The upper plots display the a priori and retrieved profiles (left) and the error budget (right). Averaging kernels and fit results (comparison between measured DSCDs and those calculated with the retrieved profile) are shown in the lower plots. Error bars on the measured DSCDs are the DOAS fit errors.

ACPD
13, 10621–10660, 2013

MAX-DOAS observations of HONO and NO_2 in the Beijing area

F. Hendrick et al.

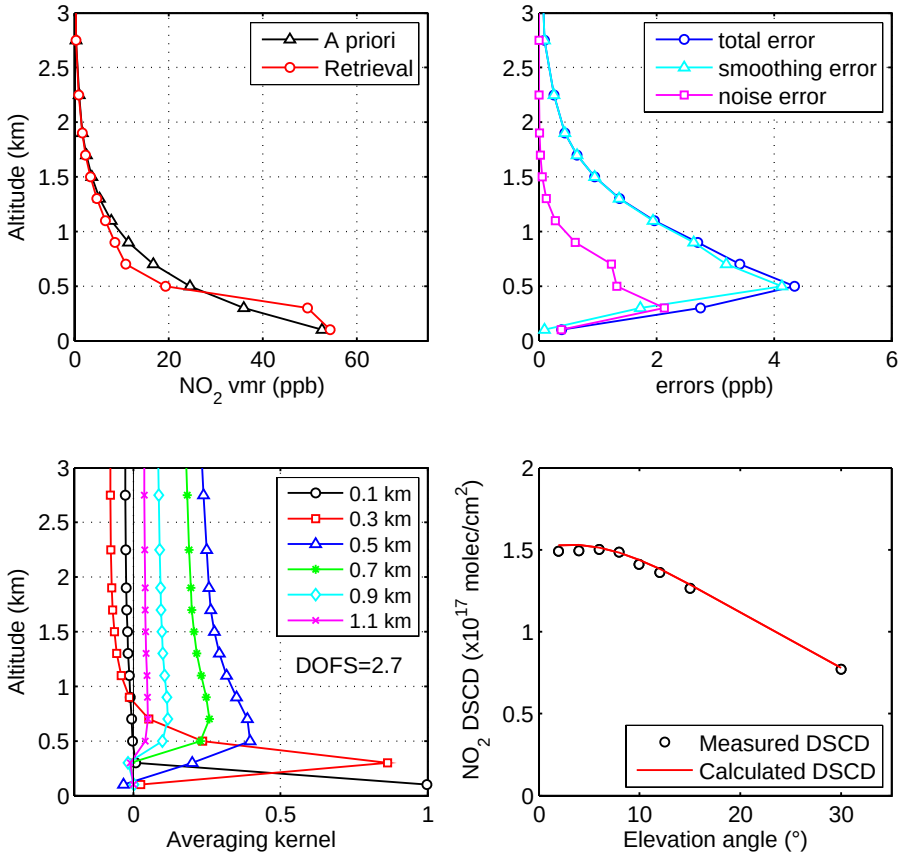

Fig. 3. Typical example of NO_2 vertical profile retrieval (Beijing, 21 January 2009, ~10:15 LT). The upper plots display to the a priori and retrieved profiles (left) and the error budget (right). Averaging kernels and fit results (comparison between measured DSCDs and those calculated with the retrieved profile) are shown in the lower plots. Error bars on the measured DSCDs are the DOAS fit errors.

ACPD
13, 10621–10660, 2013

MAX-DOAS observations of HONO and NO_2 in the Beijing area

F. Hendrick et al.

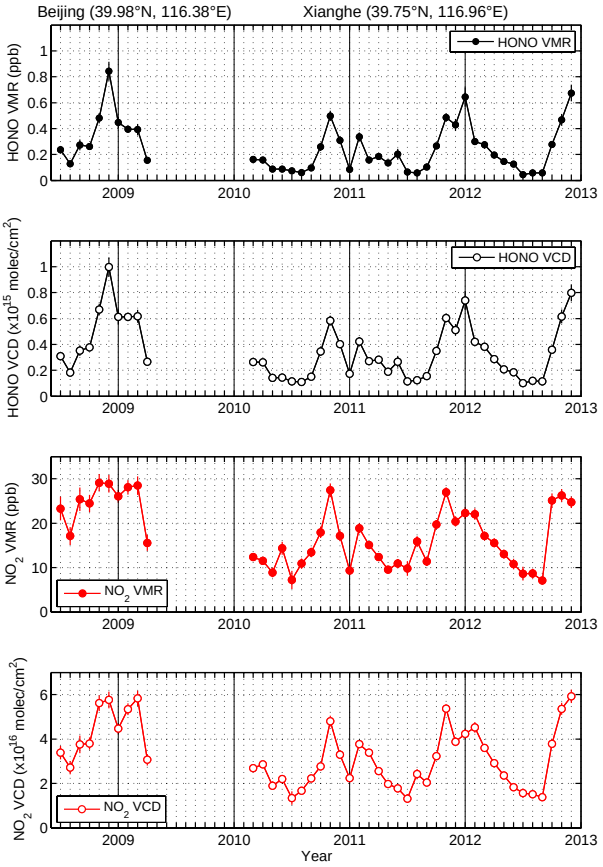

Fig. 4. Time-series of HONO and NO_2 near-surface concentrations (filled circles) and vertical columns (VCD; empty circles) at local noon at Beijing (July 2008–April 2009) and Xianghe (March 2010–December 2012). They correspond to monthly averages over the time interval of ±2 h around local noon. The error bars represent the standard deviation of the mean.

ACPD
13, 10621–10660, 2013

MAX-DOAS observations of HONO and NO_2 in the Beijing area

F. Hendrick et al.

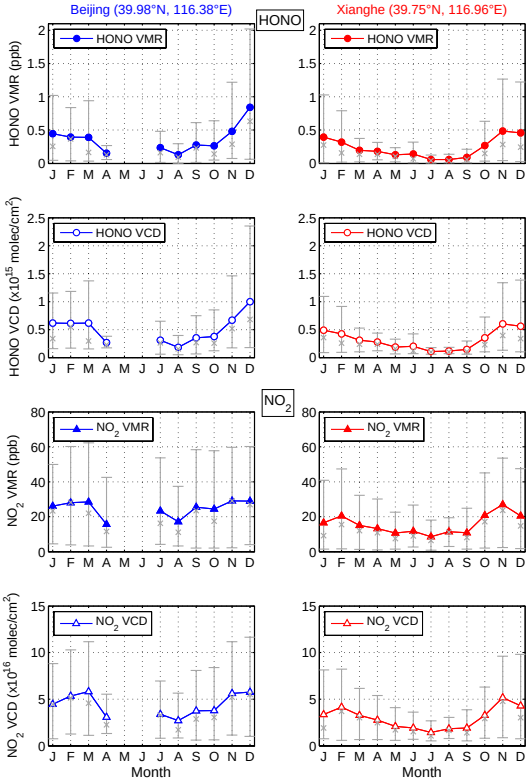

Fig. 5. Seasonal variation of the HONO and NO_2 surface concentration and vertical column density (VCD) at local noon at Beijing (left plots/blue curves) and Xianghe (right plots/red curves). Data correspond to monthly averages over the time interval of ±2 h around local noon. The cross symbol and the lower (upper) error bars represent the median and the 10th (90th) percentiles of the data, respectively.

ACPD
13, 10621–10660, 2013

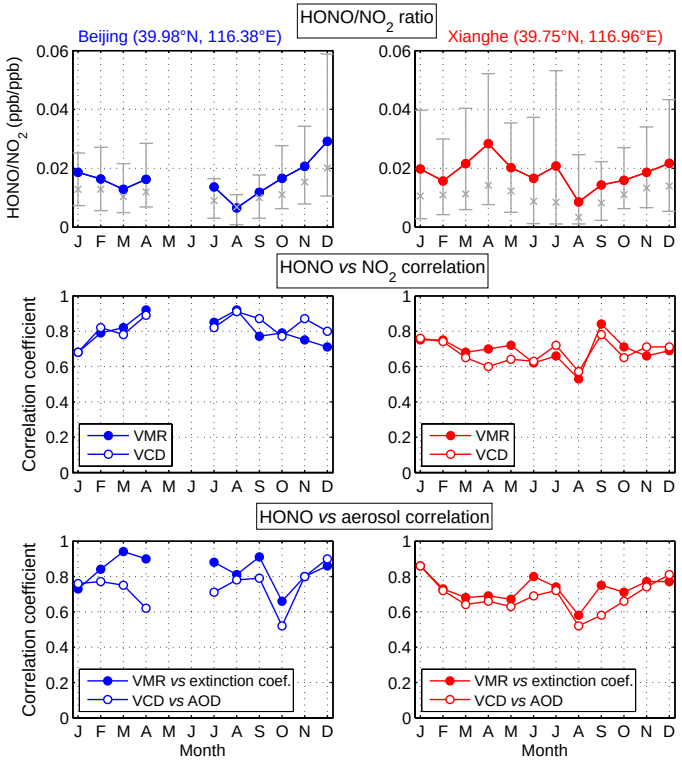

Fig. 6. Seasonal variation of the HONO to NO_2 near-surface concentration ratio, the HONO versus NO_2 correlation coefficient (0–200 m VMR and vertical column density (VCD)), and the HONO versus aerosol correlation coefficient (0–200 m VMR versus aerosol extinction coefficient and VCD versus aerosol optical depth (AOD)) at local noon at Beijing (left plots/blue curves) and Xianghe (right plots/red curves). In the upper plot, the cross symbol and the lower (upper) error bars represent the median and the 10th (90th) percentiles of the data, respectively.

ACPD
13, 10621–10660, 2013

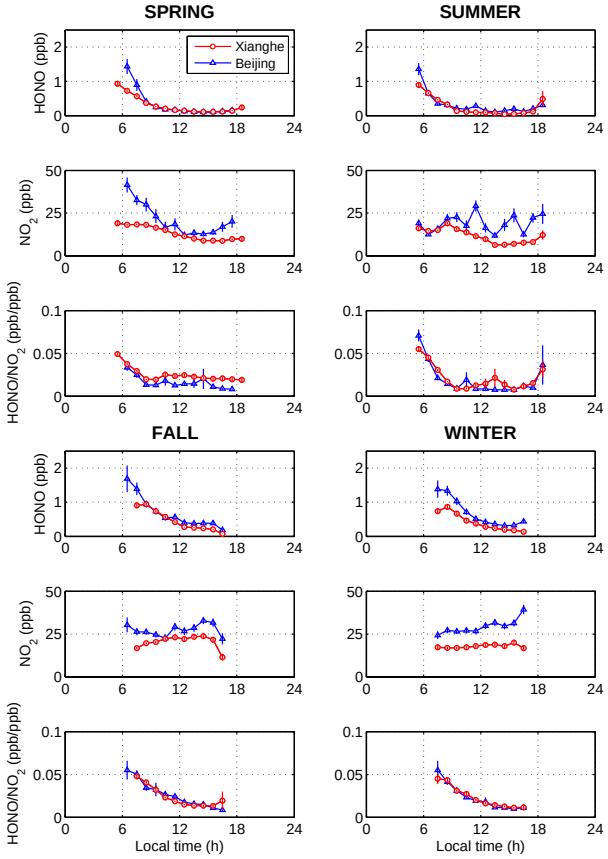

Fig. 7. Diurnal variation of the HONO and NO_2 concentrations in the 0–200 m layer and their corresponding ratio at Beijing (blue curves) and Xianghe (red curves). Data have been averaged per season using 1 h bins. The error bars correspond to the standard deviation of the mean.

ACPD
13, 10621–10660, 2013

MAX-DOAS observations of HONO and NO_2 in the Beijing area

F. Hendrick et al.

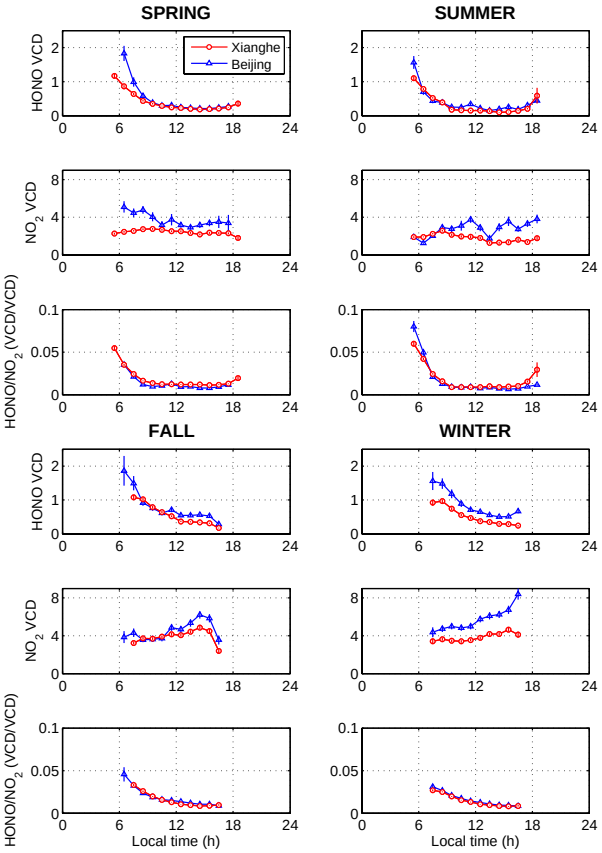

Fig. 8. Same as Fig. 8 but for the vertical column densities (VCD). HONO and NO_2 VCD are in $\times 10^{15}$ and $\times 10^{16}$ molec cm^{-2} units, respectively.

ACPD
13, 10621–10660, 2013

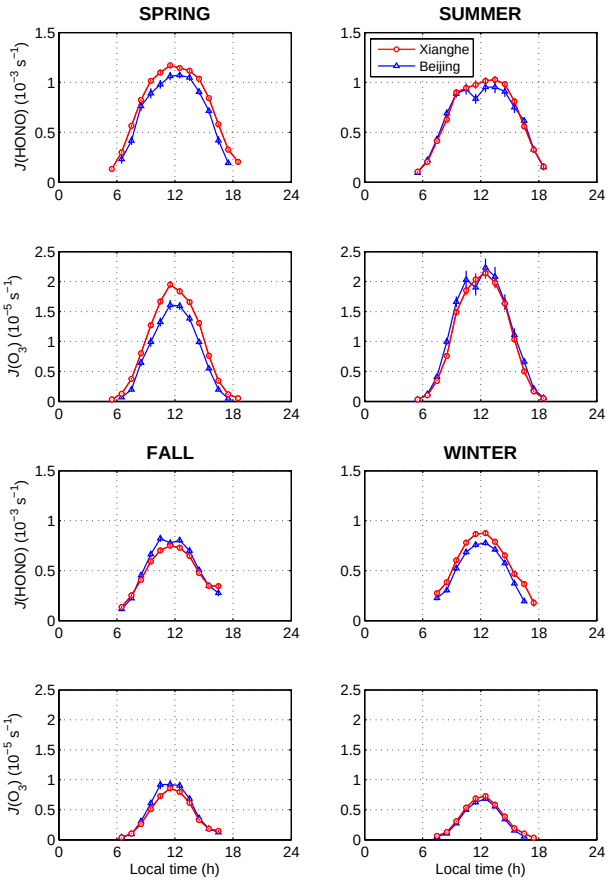

Fig. 9. Photolysis rates J (HONO) and J ($O_3 \rightarrow O(^1D)$) calculated in the 0–200 m layer for Beijing and Xianghe and averaged per season. The error bars correspond to the standard deviation of the mean.

ACPD
13, 10621–10660, 2013

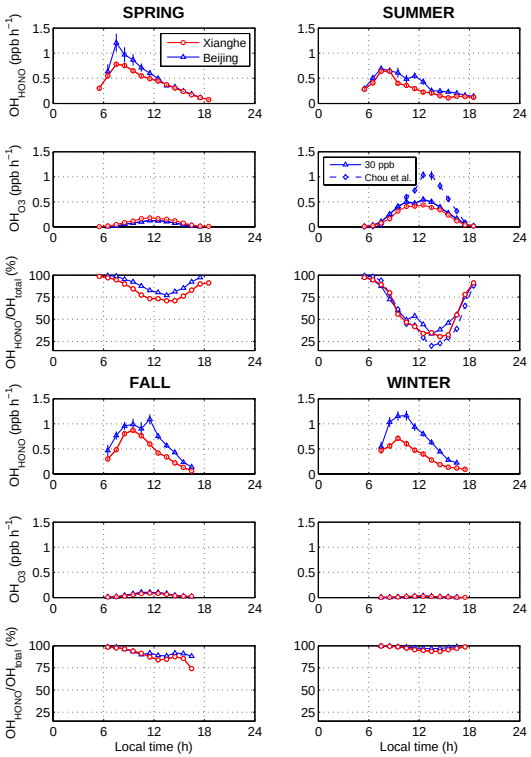

Fig. 10. Diurnal variation of the OH production from HONO (OH_{HONO}) and O_3 (OH_{O3}) in the 0–200 m layer at Beijing (blue curves) and Xianghe (red curves). Data have been seasonally averaged using 1 h bins. The relative contribution of HONO to the OH production (OH_{HONO}/OH_{total}) is calculated as follows: $OH_{HONO}/(OH_{HONO} + OH_{O3})$. The error bars correspond to the standard deviation of the mean. At Beijing in summer, the OH production from O_3 has been estimated assuming a fixed 30 ppb concentration and the diurnal cycle of O_3 measured by Chou et al. (2011).

ACPD
13, 10621–10660, 2013

MAX-DOAS observations of HONO and NO_2 in the Beijing area

F. Hendrick et al.

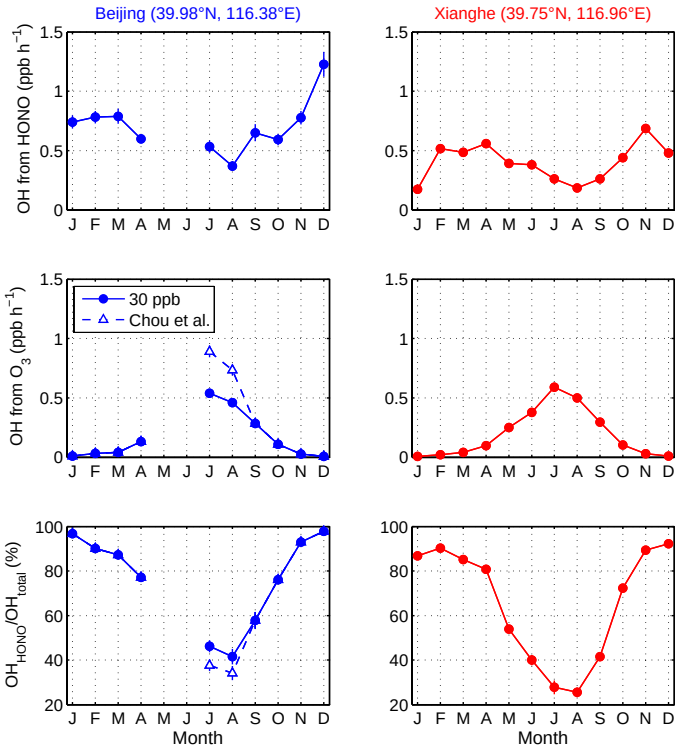

Fig. 11. Seasonal variation of the OH production from HONO (OH_{HONO}) and O_3 (OH_{O_3}) in the 0–200 m layer at Beijing (left/blue curves) and Xianghe (right/red curves) at local noon. Data correspond to monthly averages over the time interval of ±2 h around local noon. OH_{total} is equal to $OH_{HONO}+OH_{O_3}$. The error bars correspond to the standard deviation of the mean. At Beijing in summer, the OH production from O_3 has been estimated assuming a fixed 30 ppb concentration and the diurnal cycle of O_3 measured by Chou et al. (2011).

ACPD
13, 10621–10660, 2013